Broadband and fabrication-tolerant on-chip scalable mode-division multiplexing based on mode-evolution counter-tapered couplers

Jing Wang,[1,2] Yi Xuan,[2] Minghao Qi,[2] Haiyang Huang,[1] You Li,[1] Ming Li,[1] Xin Chen,[1] Zhen Sheng,[1] Aimin Wu,[1] Wei Li,[1] Xi Wang,[1] Shichang Zou,[1] and Fuwan Gan[1,*]

[1]*State Key Laboratory of Functional Materials for Informatics, Shanghai Institute of Microsystem and Information Technology, Chinese Academy of Sciences, Shanghai 200050, China*

[2]*School of Electrical and Computer Engineering and the Birck Nanotechnology Center, Purdue University, West Lafayette, Indiana 47907, USA*

**Corresponding author: fuwan@mail.sim.ac.cn*

Received January 27, 2015; revised March 23, 2015; accepted March 24, 2015; posted March 25, 2015 (Doc. ID 233256); published April 21, 2015

A broadband and fabrication-tolerant on-chip scalable mode-division multiplexing (MDM) scheme based on mode-evolution counter-tapered couplers is designed and experimentally demonstrated on a silicon-on-insulator (SOI) platform. Due to the broadband advantage offered by mode evolution, the two-mode MDM link exhibits a very large, −1 dB bandwidth of >180 nm, which is considerably larger than most of the previously reported MDM links whether they are based on mode-interference or evolution. In addition, the performance metrics remain stable for large-device width deviations from the designed valued by −60 nm to 40 nm, and for temperature variations from −25°C to 75°C. This MDM scheme can be readily extended to higher-order mode multiplexing and a three-mode MDM link is measured with less than −10 dB crosstalk from 1.46 to 1.64 μm wavelength range. © 2015 Optical Society of America

OCIS codes: (130.3120) Integrated optics devices; (230.7370) Waveguides; (030.4070) Modes; (060.4230) Multiplexing.
http://dx.doi.org/10.1364/OL.40.001956

To satisfy the rapidly increasing demands on high-speed data transfer, on-chip optical interconnections based on silicon photonics have attracted significant interest in the past few years. In addition to the wavelength-division multiplexing (WDM) technology [1], the mode-division multiplexing (MDM) has also emerged as an efficient approach to further increase the transmission capability [2]. Many MDM architectures have been proposed and experimentally demonstrated on silicon-on-insulator (SOI) platforms based on asymmetric directional coupler (ADC) [3–7], multimode interference (MMI) coupler [8–10], adiabatic coupler [11], and asymmetric Y-junction [12,13]. The ADC-based MDM takes advantage of phase-matching condition in the ADC, so its coupling length is usually short, and it can easily expand to higher order mode multiplexing as well as combine with other multiplexing schemes [3–7]. However, its performance is normally sensitive to device size variations, and the bandwidth is typically limited to a few tens of nanometers. The MMI-based MDM may have high fabrication tolerance, but its structure is relatively complicated, consisting of several MMI couplers and phase shifters [8–10]. Adiabatic couplers for on-chip two-mode MDM applications have been demonstrated recently, and they can exhibit a large bandwidth due to the broadband properties of mode evolution [11]. However, these MDM links based on MMI couplers or adiabatic couplers cannot conveniently accommodate more than two modes. Therefore their applications might be severely restricted [8–11]. The asymmetric Y-junction is a typical mode-evolution structure that has been proposed or demonstrated for WDM or MDM applications [12–16]. However, it is not easy to achieve a low-loss Y-junction corner in practice. To realize a high-performance MDM scheme, which simultaneously has large bandwidth, robust fabrication tolerance, and scalability, a counter-tapered coupler based on mode evolution has been proposed [17] and experimentally demonstrated for few-mode optical fiber network applications [18–20]. However, its application in SOI-based on-chip MDM has not been explored yet.

In this Letter, we designed and experimentally demonstrated a broadband and fabrication-tolerant on-chip scalable MDM scheme based on mode-evolution counter-tapered couplers on an SOI platform. A two-mode MDM link exhibits a −1 dB bandwidth exceeding 180 nm, which is considerably larger than most of the previously reported MDM links whether they are based on mode-interference or evolution [3–13]. In addition, its fabrication tolerance to device width deviation and scalability to higher-order modes are also characterized.

Figure 1(a) illustrates a two-mode MDM link that consists of a multiplexer and a de-multiplexer connected by a length of multi-mode transmission waveguide. The MDM link is designed in SOI strip waveguides with a 0.22-μm core height and top/bottom SiO_2 cladding. The multiplexer and de-multiplexer used for the zero-order transverse-electric/first-order transverse-electric (TE_0/TE_1) modes share the identical design parameters according to the reciprocity theorem. The operation principle in this MDM link is based on the mode evolution in a coupler that has two waveguides with cores counter tapered [17,18]. Considering that the effective mode refractive index increases with the waveguide width, there is likely a cross-point where the effective index of the mode in one taper is equal to that of another mode in the neighboring taper. This can be achieved when the waveguide widths at both sides of the tapers are properly chosen. And in such a case, certain level of mode conversion could occur. A more detailed discussion from the point of view of mode conversion between local-normal

 © 2015 Optical Society of America

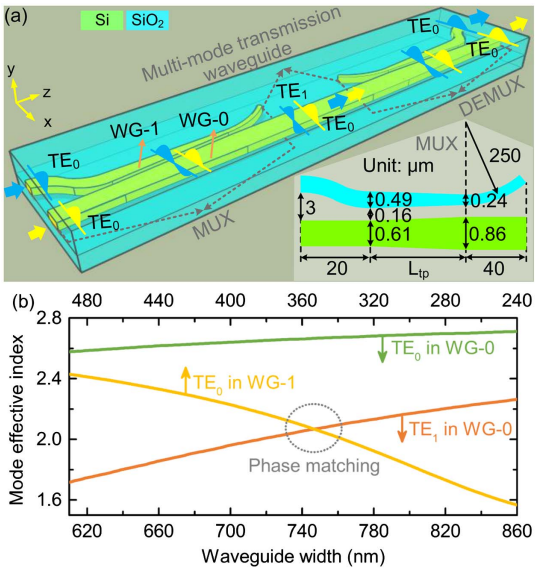

Fig. 1. (a) Schematic of the two-mode MDM link based on two counter-tapered couplers. Inset: the design parameters for the multiplexer. (b) Effective refractive index of the modes in each waveguide (WG-1/WG-0) of the coupler with width tapering from 490 nm/610 nm to 240 nm/860 nm.

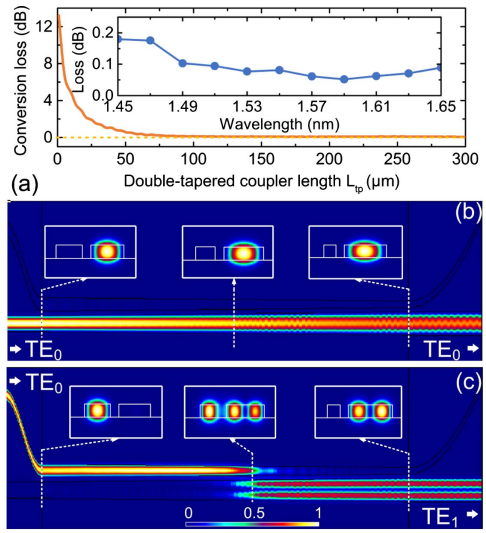

Fig. 2. (a) Mode conversion loss from the TE_0 mode in the CH1 to the TE_1 mode in the multi-mode transmission waveguide. Inset: wavelength dependence of the mode conversion loss at $L_{tp} = 200$ μm. (b) and (c) Mode propagation in the multiplexer for the input TE_0 mode from the CH0 and CH1, respectively.

modes in the counter-tapered coupler could be found in [17]. Here our entire multiplexer consists of a counter-tapered coupler sandwiched between two waveguide bends that are employed to decouple the light coupling and also to reduce the radiation loss at both ends of the multiplexer. The upper waveguide (named a WG-1) of the coupler has a width varying from 0.49 to 0.24 μm, whereas the bottom waveguide (named as WG-0) has a width increasing from 0.61 to 0.86 μm. We used a commercial software, FIMMWAVE, to calculate the effective refractive indices of the TE_0 mode and the TE_1 mode in WG-0 and that of the TE_0 mode in WG-1 at 1.55-μm wavelength. Figure 1(b) shows that there is a cross-point or phase-matching point for the TE_1 curve of WG-0 and the TE_0 curve of WG-1, which means the input TE_0 mode in the WG-1 could adiabatically convert to the TE_1 mode in the adjacent WG-0 if the coupler length L_{tp} is large enough. However, since the TE_0 curve of WG-0 has no intersection with other curves, the incoming TE_0 mode to the WG-0 would remain propagating along this waveguide without any conversion to other modes. The width difference between both sides of the tapers is chosen as 0.25 μm to ensure a large difference of effective indices, and thus the converted mode will not be coupled back. A lower width difference may cause some unwanted mode interference or radiation, whereas a larger one would probably increase the device length. After the TE_0 mode and the TE_1 mode are multiplexed in the counter-tapered coupler, they will transmit in the multi-mode transmission waveguide and subsequently get de-multiplexed to different output ports in the de-multiplexer.

We further used a 3D simulation software, FIMMPROP, to calculate the mode conversion loss in the overall multiplexer, and the parameters used in the simulation are shown in the inset of Fig. 1(a). Figure 2(a) shows the mode conversion loss from the input TE_0 mode in the upper port (denoted as CH1) to the TE_1 mode in the bottom output port at 1.55-μm wavelength. The mode conversion loss in the multiplexer decreases when the taper length increases, and a very low loss of <0.1 dB can be achieved when $L_{tp} > 120$ μm. Here we chose $L_{tp} = 200$ μm to ensure a good trade-off between a low loss and a small footprint. In addition, the multiplexer shows broadband properties in the wavelength range from 1.45 to 1.65 μm where the mode conversion loss remains lower than 0.18 dB.

Figures 2(b) and 2(c) show the calculated mode propagation in the multiplexer for the TE_0 mode from the bottom input port (denoted as CH0) and CH1, respectively, demonstrating the mode conversion as we expected. When the input TE_0 mode is from port CH0, it passes through the multiplexer with negligible power transferred to the adjacent waveguide. And the power of the input TE_0 mode from the CH0 will gradually couple to the bottom waveguide and finally output as the TE_1 mode.

This MDM link was fabricated on an SOI wafer with 2-μm-thick buried oxide and a top silicon layer of 220 nm. The devices were patterned with electron-beam lithography and then over-cladded with 2-μm-thick low temperature oxide. Figure 3 shows the microscope photos of this two-mode MDM link and its reference waveguide. The devices were measured in a butt-coupling setup. The light from a tunable laser source was adjusted by a polarization controller and then coupled to the devices by a lensed fiber. The output light passing through another lensed fiber was collected by a power detector to characterize the transmission properties. Before measuring the devices, a broadband polarization beam-splitting prism was used to calibrate the input TE_0 polarization with a polarization extinction ratio ~20 dB to the zero-order transverse-magnetic (TM_0) mode.

Figure 4(a) shows the normalized transmission characteristics of the designed two-mode MDM link. Here we

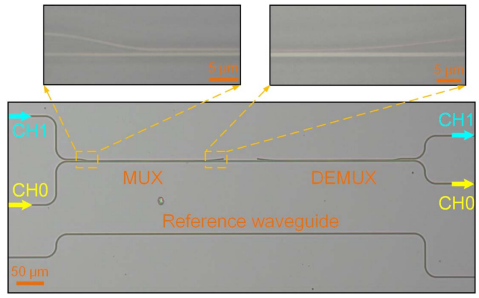

Fig. 3. Microscope photos of the two-mode MDM link with a ~60 μm-long multi-mode waveguide.

define T_{ij} as the transmission characteristics of the TE_0 mode from the CHi to the CHj. The excess loss of the TE_0 link (i.e., $-T_{00}$) and TE_1 link (i.e., $-T_{11}$) are 0.41 and 0.74 dB at 1.55-μm wavelength, respectively. T_{11} is slightly lower than T_{00} because the TE_1 link requires double-mode conversion, while the TE_0 link is similar to a long waveguide without any mode conversion. In addition, T_{00} has a larger bandwidth than T_{11}, and only ~0.5 dB loss variation is achieved from 1.46 to 1.64 μm wavelength range. Nevertheless, T_{11} still has a −1 dB bandwidth of >180 nm, limited by the wavelength range of tunable laser source. The MDM link also exhibits a low crosstalk of −25.5 dB and −26.1 dB at 1.55-μm wavelength for the CH1 and CH0 input, respectively. The crosstalk performance degrades slightly at other wavelengths, partially due to the polarization variation from the tunable laser source [7]. However, crosstalk less than −13 dB could be achieved across a 180-nm wavelength range for both two inputs.

To analyze the fabrication tolerance of this MDM link, we fabricated two samples with waveguide width deviation of $\Delta w = -60$ nm and $\Delta w = 40$ nm, respectively. Figures 4(b) and 4(c) show the normalized transmission characteristics of these two samples, respectively. The performance degradation is very small even for such a large size variation, and both devices still exhibit large operating bandwidth. This can be attributed to the advantages of mode evolution. Some ripples in the T_{11} curves

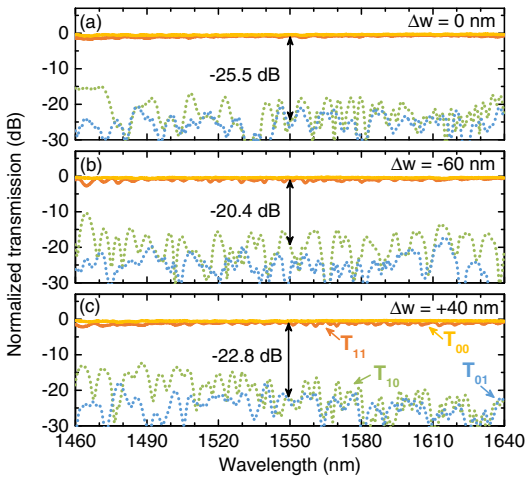

Fig. 4. Normalized transmission characteristics of the MDM link with (a) designed coupler sizes, and the width deviations of (b) $\Delta w = -60$ nm and (c) $\Delta w = 40$ nm.

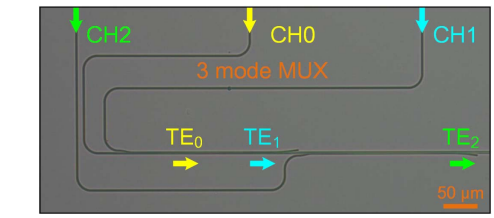

Fig. 5. Microscope photos of the three-mode mode-division multiplexer.

are observed, possibly due to some unwanted mode interference in the counter-tapered couplers. We believe such a large fabrication tolerance could significantly improve the manufacture yield.

This MDM scheme based on counter-tapered coupler can be readily extended to high-order mode multiplexing, showing advantage over other mode-evolution-based MDM schemes [11]. Figure 5 shows the microscope photo of a three-mode mode-division multiplexer designed for TE_0, TE_1, and second-order transverse-electric (TE_2) modes. The multi-mode transmission waveguide and corresponding de-multiplexer are not shown here. The three-mode multiplexer has the same design parameters for the TE_0/TE_1 multiplexing part as the one shown in the inset of Fig. 1(a). The design parameters in the TE_2 multiplexing part can be obtained by calculating the effective refractive indices of the TE_0 mode in the upper waveguide and the TE_2 mode in the bottom waveguide. When the upper/bottom waveguide has a width varying from 0.4 μm/1 μm to 0.2 μm/1.2 μm, somewhere along the taper there will be a cross-point, which will cause the TE_0 mode in the upper waveguide to be converted to the TE_2 mode in the bottom waveguide. The taper length in this part is chosen to be 200 μm.

Figures 6(a)–6(c) show the total transmission characteristics of the three-mode MDM link for different input channels, respectively. The crosstalk for the input from CH0, CH1, and CH2 are −20.5 dB, −15.9 dB, and −14.4 dB, respectively. Even though the performance is degraded when the number of multiplexed modes

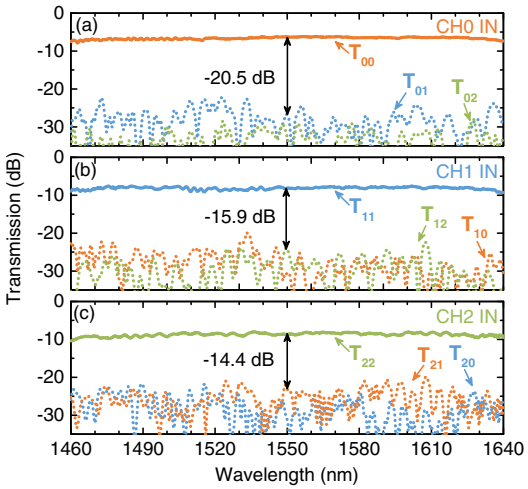

Fig. 6. (a)–(c) Transmission characteristics of the three-mode MDM link when the input channel is CH0, CH1, and CH2, respectively.

increases, ≤10 dB crosstalk is achieved for a wavelength range of 1.46–1.64 μm, showing potential for broadband hybrid multiplexing schemes together with WDM and polarization-division multiplexing (PDM) [4–8]. We believe it is highly feasible to extend this MDM scheme to higher order mode multiplexing when each multiplexer is carefully optimized.

In addition to the mode conversion loss in this MDM link, the propagation loss also contributes considerably to the total loss, especially when the multiplexer/demultiplexer length is relatively large. This loss could be improved by optimizing the fabrication process [21]. Moreover, the butt-coupling may induce some Fabry–Perot reflection at the facet between the fiber and waveguide and cause some other unwanted input polarizations, which will lead to a relatively high crosstalk. A potential solution is to use the grating-coupling instead of butt-coupling, and the grating coupler can work as a polarization filter to significantly improve the crosstalk performances [5].

We have also simulated the mode-conversion efficiency degradation due to the temperature variation. When the temperature changes from −25°C to 75°C, the refractive index of Si increases approximately from 3.4678 to 3.4861 at 1550-nm wavelength. However, the effective indices of the upper and bottom waveguide will change, relatively, by a similar amount. Therefore, the index variation caused by the temperature cannot significantly alter the cross-point of the TE_0 and TE_1 curves as shown in Fig. 1(b), and a high efficiency can still be achieved when the coupler length is large enough. As a result, there is only <0.5% variation for the mode conversion efficiency from the TE_0 mode from the upper input waveguide to the TE_1 mode in the multi-mode transmission waveguide.

In summary, we have demonstrated a broadband and fabrication-tolerant on-chip scalable MDM scheme based on mode-evolution counter-tapered couplers on an SOI platform. The mode multiplexing in the counter-tapered coupler is analyzed, and the coupler length is optimized to reduce the mode conversion loss. The measurement results show that the two-mode MDM link has a −1 dB bandwidth of >180 nm with −13 dB crosstalk in a wavelength range from 1.46 to 1.64 μm. And the performance remains stable even for a large device width deviation from −60 nm to 40 nm. This MDM scheme can be readily extended to higher order mode multiplexing, and a three-mode MDM link is demonstrated with less than −10 dB crosstalk in the 180-nm wavelength range. We believe this MDM can be potentially integrated with other multiplexing schemes like WDM and PDM to further increase the transmission capability in optical interconnects and communications.

This work was partially supported by the Science and Technology Commission of Shanghai Municipality (No. 14JC1407600), the State High-Tech Development Plan (No. 2012AA012202), and the National Natural Science Foundation of China (Nos. 61106051, 61107031, 61275112, and 61475180). M. Qi and Y. Xuan were partially supported by the National Science Foundation grants CMMI-1120577 and CNS-1126688, National Institute of Health grant 1R01RR026273-01, and Defense Threat Reduction Agency grant HDTRA1-10-1-0106. M. Qi acknowledges partial support from CAS International Collaboration and Innovation Program on High Mobility Materials Engineering.

References

1. S. Pathak, D. Thourhout, and W. Bogaerts, Opt. Lett. **38**, 2961 (2013).
2. R. van Uden, R. Correa, E. Lopez, F. Huijskens, C. Xia, G. Li, A. Schulzgen, H. de Waardt, A. Koonen, and C. Okonkwo, Nat. Photonics **8**, 865 (2014).
3. D. Dai, J. Wang, and Y. Shi, Opt. Lett. **38**, 1422 (2013).
4. L. Luo, N. Ophir, C. Chen, L. Gabrielli, C. Poitras, K. Bergmen, and M. Lipson, Nat. Commun. **5**, 3069 (2014).
5. J. Wang, P. Chen, S. Chen, Y. Shi, and D. Dai, Opt. Express **22**, 12799 (2014).
6. J. Wang, S. Chen, and D. Dai, Opt. Lett. **39**, 6993 (2014).
7. J. Wang, S. He, and D. Dai, Laser Photon. Rev. **8**, L18 (2014).
8. M. Ye, Y. Yu, J. Zou, W. Yang, and X. Zhang, Opt. Lett. **39**, 758 (2014).
9. T. Uematsu, Y. Ishizaka, Y. Kawaguchi, K. Saitoh, and M. Koshiba, J. Lightwave Technol. **30**, 2421 (2012).
10. Y. Li, C. Li, C. Li, B. Cheng, and C. Xue, Opt. Express **22**, 5781 (2014).
11. J. Xing, Z. Li, X. Xiao, J. Yu, and Y. Yu, Opt. Lett. **38**, 3468 (2013).
12. J. Driscoll, R. Grote, B. Souhan, J. Dadap, M. Lu, and R. Osgood, Opt. Lett. **38**, 1854 (2013).
13. J. Driscoll, C. Chen, R. Grote, B. Souhan, J. Dadap, A. Stein, M. Lu, K. Bergman, and R. Osgood, Jr., Opt. Express **22**, 18543 (2014).
14. W. Henry and J. Love, Opt. Quantum Electron. **29**, 379 (1997).
15. J. Love and A. Ankiewicz, Electron. Lett. **39**, 1385 (2003).
16. W. Chen, P. Wang, and J. Yang, Opt. Express **21**, 25113 (2013).
17. F. Milton and W. Burns, Appl. Opt. **14**, 1207 (1975).
18. N. Riesen and J. Love, J. Lightwave Technol. **31**, 2163 (2013).
19. N. Riesen and J. Love, IEEE Photon. Technol. Lett. **25**, 2501 (2013).
20. S. Gross, N. Riesen, J. Love, and M. Withford, Laser Photon. Rev. **8**, L81 (2014).
21. C. Qiu, Z. Sheng, H. Li, W. Liu, L. Li, A. Pang, A. Wu, X. Wang, S. Zou, and F. Gan, J. Lightwave Technol. **32**, 2303 (2014).

210.28.139.179 (as 2022-07-04 08:26:10)